Hindawi
International Journal of Corrosion
Volume 2019, Article ID 9506401, 9 pages
https://doi.org/10.1155/2019/9506401

Research Article

Effect of Aging Treatment on Intergranular Corrosion Properties of Ultra-Low Iron 625 Alloy

Zhi-yuan Zhu,[1] **Yi Sui**,[1] **An-lun Dai**,[1] **Yuan-fei Cai**,[1] **Ling-Li Xu**,[1] **Ze-xin Wang**,[1] **Hong-mei Chen**,[1] **Xing-ming Shao**,[2] **and Wei Liu**[2]

[1] *School of Materials Science and Engineering Jiangsu University of Science and Technology, Zhenjiang, Jiangsu 212003, China*
[2] *Jiangsu Xinhua Alloy Electric Co., Ltd., Xinghua, Jiangsu 225722, China*

Correspondence should be addressed to Zhi-yuan Zhu; salanganezhu@163.com

Received 3 August 2018; Accepted 6 December 2018; Published 2 January 2019

Guest Editor: Xiang Li

The microstructures evolution of precipitations for an ultra-low iron Alloy 625 subjected to long term aging treatment at 750°C was investigated using scanning electron microscope (SEM) and X-ray diffraction (XRD). The intergranular corrosion behaviors of Alloy 625 were evaluated by using ASTM G28A. The result shows that the precipitated phase γ''-Ni_3Nb was mainly precipitated at the grain boundaries and twin boundaries. The number and volume fraction of γ'' increased with the prolonging of aging time. The transformation of γ'' to δ-Ni_3Nb occurred after aging periods of 200 h. The corrosion resistance of Alloy 625 was significantly reduced during aging treatment. The decrease in intergranular corrosion resistance of Alloy 625 was attributed to the dissolution of precipitated phase and chromium depleted zone. The mass loss rate of Alloy 625 after aging treatment is related to the volume of precipitated phase and can be simulated by Johnson-Mehl-Avrami equation.

1. Introduction

Because of the excellent properties such as good strength, ductility and toughness, welding, and corrosion resistance, nickel-base alloy is widely used in naval architecture and ocean engineering, petroleum refining and petrochemical industries, and energy and power industry [1–3]. As a kind of nickel-based alloy, Alloy 625 seems to be the suitable material used in the 4th generation of nuclear power systems [4, 5] owing to its attractive features. Alloy 625 has the problem of precipitateγ''-Ni_3Nb and carbide [6–9] in high temperature by long term aging. The aging and creep properties of alloys are important parameters for safety operation of component made of Alloy 625. During the long term aging, the γ'' phase can gradually transformed into needle-like δ-Ni_3Nb leading to the increasing of the hardness [10] and decreasing of the ductility and toughness. Because of its high potential, preferential corrosion usually occurs on Ni_3Nb in oxidizing media. At the same time, intergranular corrosion can also occur in the area of carbide and chromium-depleted zone at grain boundaries [11–14]. However, the work concentrated on the effect of formation and transformation of precipitated phase on corrosion behaviour of nickel-based alloy during the long term aging is rarely reported.

Commercial Alloy 625 usually contains 2-5% wt Fe and Fe atoms are present in the matrix in solid solution. The Topological Close-Packed Phase such as Laves phase, μ phase, and σ phase [15], as shown in Table 1, will be precipitated in the long aging. These phases are plate-shaped or needle-shaped, leading to the reduction of fracture strength and plasticity [16]. In addition, Si can also facilitate the precipitation of harmful phase [17] leading to the decrease of the service life of components.

The aim of present study was focused on the effect of aging treatment on precipitation behaviour and intergranular corrosion properties of a newly developed ultra-low iron Alloy 625.

2. Experimental

The Alloy 625 used in present work is provided by Jiangsu XinHua Alloy Electric CO., LTD., the composition of which

Table 1: The main phases occurring in long-term aging nickel-based superalloy.

Phase	Structure	Typical Composition
γ''	body-centered tetragonal	$Ni_3(Nb_{>0.5},Ti_{<0.5},Al_{<0.5},Mo_{<0.5})$
δ	orthorhombic	Ni_3Nb
MC	cubic	(Nb,Ti)C
M_6C	cubic	$(Cr_{>0.2},Mo_{>0.2},Fe)C$
$M_{23}C_6$	cubic	$(Cr_{>0.8},Fe,Mo)C$
Laves	$MgZn_2$-Types(AB_2)	$TiFe_2$, $NbFe_2$, $MoFe_2$, etc.
μ	Hexagonal(B_7A_6)	Fe_7Mo_6, Fe_7Nb_6, Fe_7Mo_6, etc
σ	Tetragonal(BA)	$(Cr,Mo)_x(Ni,Fe)_y$: FeCr, MoFe, NbFe, etc.

Table 2: Chemical composition of Alloy 625 (wt%).

C	Cr	Mo	Co	Nb+Ta	Fe	Al	Ti	Si	P	S	Ni
0.05	22.4	9.5	0.03	3.66	0.01	0.24	0.23	0.04	0.002	0.001	63.1

is listed in Table 2. The microstructure of Alloy 625 is shown in Figure 1. It can be seen that Alloy 625 has a single-phase austenite with carbide particles (black cross) distributed on the surface. The specimens of $50 \times 24 \times 5$ (± 0.3) mm for intergranular corrosion investigations were machined from the hot rolled sheets. All the specimens were solution annealed at 1140°C for 4.5 h in an argon protective atmosphere followed by water quenching. Stabilizing treatment was performed at a temperature of 1000°C for 6.5 h in an evacuated tube and cooling to room temperature in air. Aging treatment was conducted at a temperature of 1000°C 750°C for 40 h, 200 h, and 1000 h. Electrolytic etching with 10% oxalic acid solution was used to reveal the microstructure in the present study.

Intergranular corrosion tests were carried out in glass container containing 236 mL H_2SO_4, 25g reagent grade ferric sulfate (containing about 75 % $Fe_2(SO_4)_3$), and 400 mL water according to ASTM G28A-02 [18]. The test was carried out in the boiling solution and the testing duration was 120 h. All the specimens for immersion tests were weighed using analytical balance with sensitivity of 0.01 mg before and after corrosion tests. The mass loss rate (mpy), with units of mm/year, was calculated as follows.

$$\text{mpy} = \frac{\Delta W}{\rho S t} \times 24 \times 365 \quad (1)$$

where ΔW is the weight loss of specimens (g), ρ is the density of the stainless steels (g/mm^3), S is the total corrosion area (mm^2), and t is the time of exposure (h).

After metallographic etching or intergranular corrosion tests, the specimens were rinsed with deionized water and alcohol and then dried. The microstructural characteristics and intergranular corrosion morphologies were examined using a scanning electronic microscope (SEM, Zeiss MERLIN) equipped with an energy dispersive spectrum analyzer. The phase analysis was performed using an X-ray diffraction (XRD, D8 Advance A25X) analyzer.

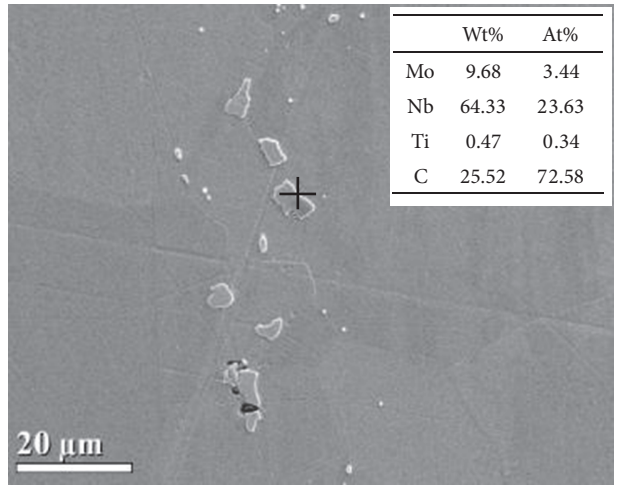

Figure 1: Microstructure of solution alloy by means of SEM.

3. Result and Discussion

3.1. Microstructure Characterization. The composition of the precipitated phase in Figure 2(b) was analyzed using the energy dispersive X-ray (EDX). Figures 2(a) and 2(b) show the morphology of Alloy 625 after stabilized treatment. It can be seen that, after the stabilized treatment, the carbide is preferentially precipitated at the grain boundary and twin boundary. Discontinuous and irregular precipitated phase distributed in grain boundary is (Mo, Nb)C. The precipitated phase at the triple line boundary is (Nb,Ti)C. In addition, a localized enrichment of C and Nb was observed at the grain boundaries in Figures 2(b), 3(a), 2(h) and 3(b). In the subsequent aging process, these carbide particles can prevent the migration of grain boundary. However, there is also the nucleation site for the precipitated phase. After 40 h aging treatment, granular like γ''-Ni_3Nb phases are present at the grain boundary and twin boundary, as shown in Figures 2(c) and 2(d). With the increasing of aging time, the density of metastable γ'' phase increases, the coarsening of which occurred. The metastable γ'' phase gradually transforms to the stable δ phase. After 200 h aging treatment, the needle-like δ is preferentially precipitated at the grain boundary and then grown into the inside of the grain, as shown in Figures 2(c) and 2(d). Also, γ'' is continuously precipitated in the grain and coursing. The number of needle-like δ phases increased significantly after 1000 h aging treatment, as shown in Figure 2(g). Also, γ'' phase can be observed inside the grains.

The precipitated phase of Alloy 625 during aging sensitization at 750°C for different time was determined by X-ray diffraction (XRD), the composition of which is listed in Table 3. The XRD profiles of Alloy 625 after aging sensitization for different time are shown in Figure 4. From Figure 4, it can be seen that the peak appeared at 35.0° and 40.7° corresponding to the diffraction peak of NbC after stabilization. After 40h of aging, the peak appeared at 42.3° corresponding to the diffraction peak of γ''-Ni_3Nb. Because the amount of precipitation was small, the peak intensity

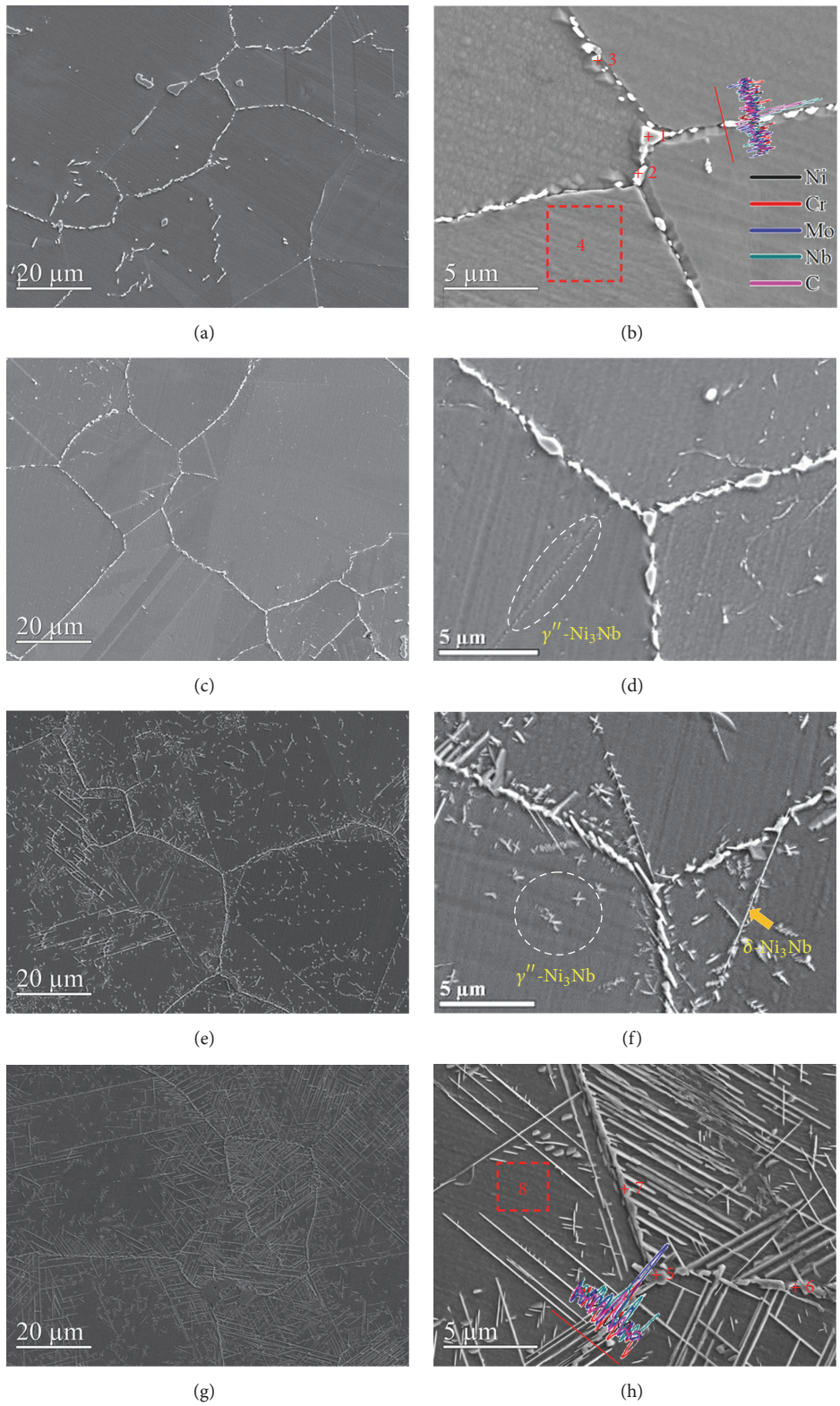

Figure 2: Microstructure of Alloy 625 after aging sensitization for different times. (a),(b) 0h; (c),(d)40h; (e), (f)200h; (g),(h)1000h.

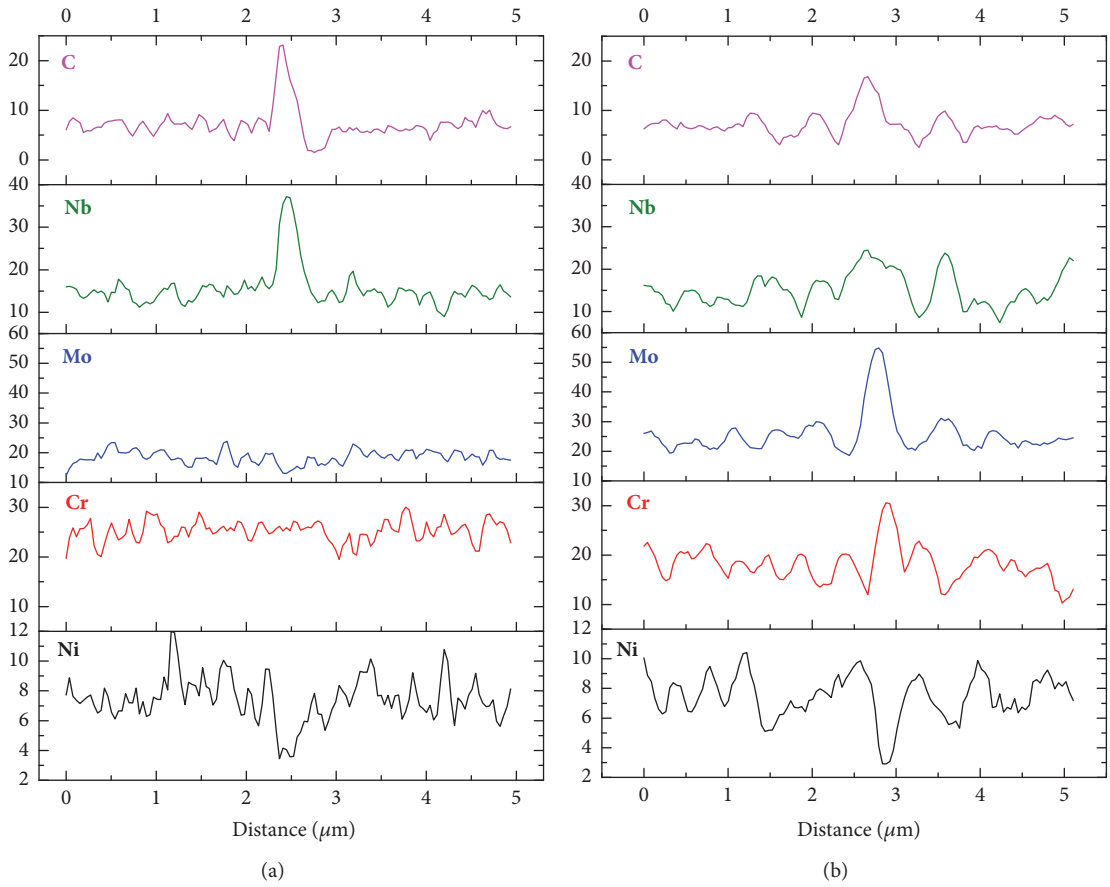

Figure 3: EDS analysis of the area marked in Figure 2. (a) 0h aging sensitization. (b)1000h aging sensitization.

Table 3: Composition at some topical points, as obtained by EDS analysis (wt%).

Position	Ni	Cr	Mo	Nb	Ti	C
1	57.03	13.57	8.33	11.89	1.70	7.47
2	58.50	15.25	8.84	10.00	2.18	5.22
3	55.79	15.75	13.01	7.60	-	7.85
4	67.11	17.91	7.78	3.57	-	3.62
5	41.42	39.35	8.83	-	2.31	8.09
6	65.59	7.54	8.56	9.97	2.56	5.77
7	41.65	16.00	30.22	2.42	-	9.71
8	67.51	17.43	7.64	2.37	-	5.04

is relatively weak. The intensity for the diffraction peak of Ni_3Nb increases with the increases of aging time. The results shown in Figure 4 are consistent with the results obtained in Figure 2.

3.2. Intergranular Corrosion Test. Figure 5 shows the mass loss of Alloy 625 specimens after the 120h ferric sulfate-sulfuric acid corrosion test (i.e., ASTM- G28A-02). It can be seen that the weight loss during corrosion increases with aging time. The mass loss rate of Alloy after stabilization treatment is 1.27mm/a. After aging for 40 h, 200 h, and 1000 h, the weight loss rate is 50.86 mm/a, 64.51 mm/a, and 87.17 mm/a, respectively. Although the aging treated samples have higher corrosion rates than the stabilization treatment, they have lower corrosion rates suggesting a rapid formation of the passivation film on the sample surface. The relationship between mass loss rate and aging time can be fitted as follows:

$$mpy = 90.20 - 44.32 \exp\left(-\frac{t}{10.99}\right) - 44.52 \exp\left(-\frac{t}{327.8}\right) \quad (2)$$

The surface morphologies of the Alloy 625 specimens after aging at 750°C for different time in ferric sulfate-sulfuric acid test for 120 h are presented in Figure 5. Only a few numbers of grain boundaries have been found to be corroded in the stabilization treated specimen; cankerous attack patterns appeared frequently along the grain boundaries, as shown in Figure 6(a). In contrast to Figure 6(a), most of the grain boundaries are completely corroded for the specimen after aging for 40 h, as envisaged from Figure 6(b). Actually, for the aging treated sample, the intergranular corrosion propagates along grain boundaries from the surface into the material interior and causes mass loss due to grain dropping, as shown in Figure 6(c). Thereafter, the corrosion rate is accelerated with the drop of the grains. Very fine cellular-like patterns could be observed on the surface (Figure 6(e)), seemingly

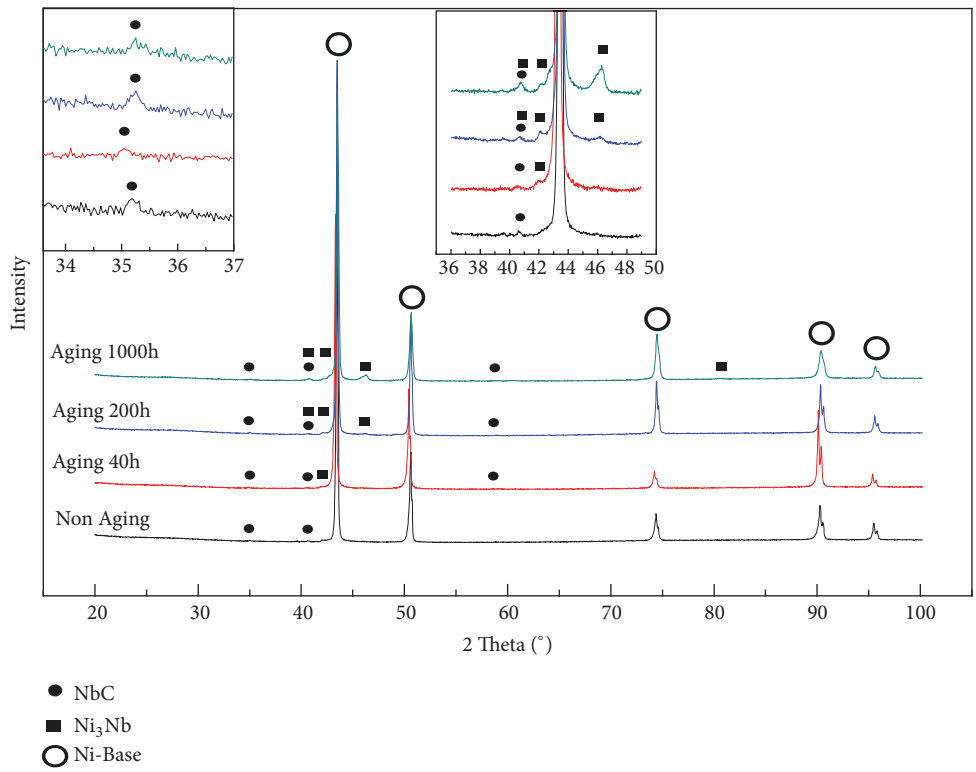

Figure 4: XRD profiles of Alloy 625 after aging sensitization for different time.

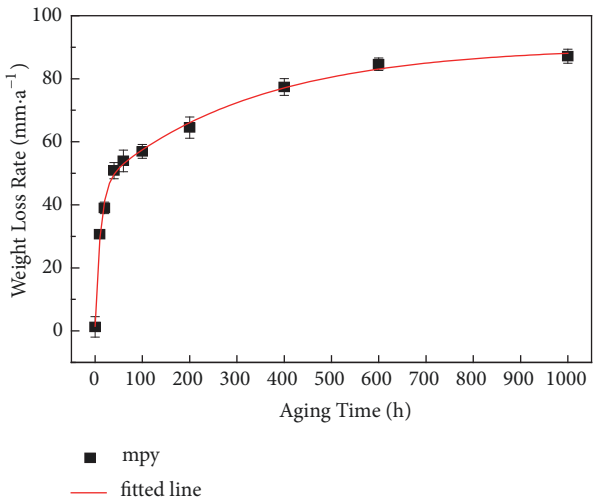

Figure 5: Mass loss rate of Alloy 625 as a function of aging time.

suggesting a preferential dissolution of Ni_3Nb. With the increase of aging time, the surface grains have completely dropped, as shown in Figure 6(d), and correspondingly the corrosion rate rapidly increases. Note that the Alloy 625 specimen exhibits two types of precipitation phase: one is the detached needle like γ''-Ni_3Nb from the surface, and the other is the detached lamellar like δ-Ni_3Nb, as indicated by the red and yellow arrows in Figure 6(f), respectively.

The cross-sectional SEM images of the Alloy 625 after immersing corrosion for 120 h are shown in Figure 7. SEM imaging of cross-sections (Figure 7) further confirms the results of Figure 6. The stabilization treated sample displays a relative flat surface and only one big intergranular corrosion crack occurs on the surface, as shown in Figure 7(a). The crack originated from the area of carbide at the grain boundary and spread along the grain boundaries into the interior of the material. The aging treated specimens exhibit an obvious intergranular corrosion, as shown in Figures 7(b), 7(c), and 7(d). The comparison of cross-sections in Figure 7 effectively makes further confirmation on the deterioration of intergranular corrosion by the aging treatment method in the tested alloy.

4. Discussion

Cr and Mo can combine with carbon elements to form carbides which are continuously precipitated at the grain boundary during long term aging treatment. The dilution zone of Cr and Mo can form adjacent to the grain boundary because the diffusion rate of Cr and Mo is far lower than that of carbon. The widths of the depleted zone and the amount of precipitates can be calculated by using Fick's second law [19]:

$$\frac{\partial C}{\partial t} = D\frac{\partial^2 C}{\partial x^2} \tag{3}$$

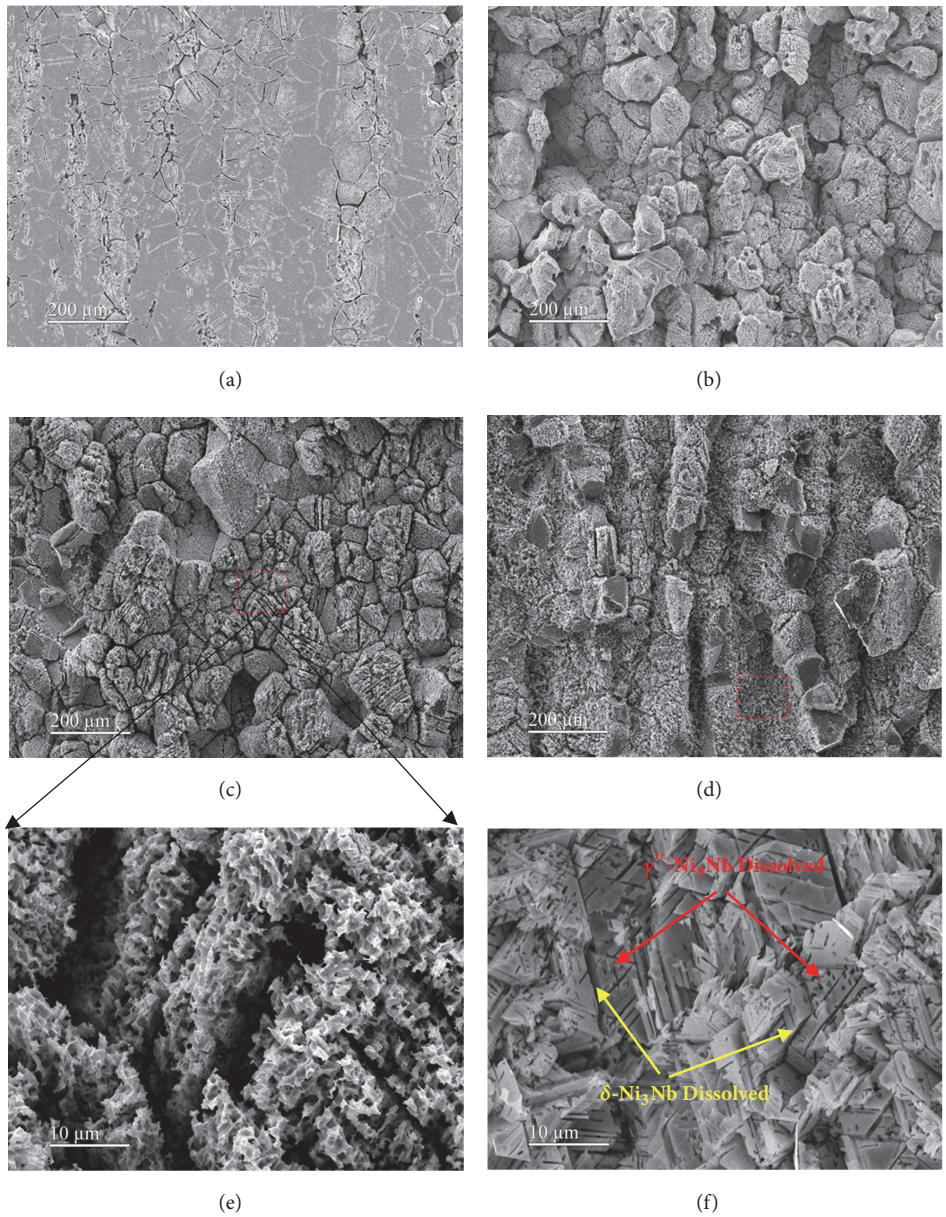

Figure 6: SEM morphologies showing the microstructure of Alloy 625 after aging for (a) 0h; (b) 40h; (c),(e) 200h; and (d),(f) 1000h.

Initial and boundary conditions:

$$t = 0,$$
$$\begin{cases} C = C_P, & x = 0 \\ C = C_G^0, & x > 0; \end{cases}$$
$$t > 0, \tag{4}$$
$$\begin{cases} C = C_P, & x = 0 \\ C = C_G^0, & x = +\infty. \end{cases}$$

The solution of the equation can be obtained by using Boltzmann Transformation and Gauss Error Function:

$$C(x,t) = C_P + \left(C_G^0 - C_P\right) \bullet \frac{2}{\sqrt{\pi}} \int_0^{\beta} \exp\left(-\beta^2\right) d\beta, \quad \left(\beta = \frac{x}{2\sqrt{Dt}}\right) \tag{5}$$

$$C(x,t) = C_P + \left(C_G^0 - C_P\right) \operatorname{erf}\left(\frac{x}{2\sqrt{Dt}}\right) \tag{6}$$

where C_P is precipitation phase of grain boundary and alloy element concentration of substrate's interface; nonsensitized

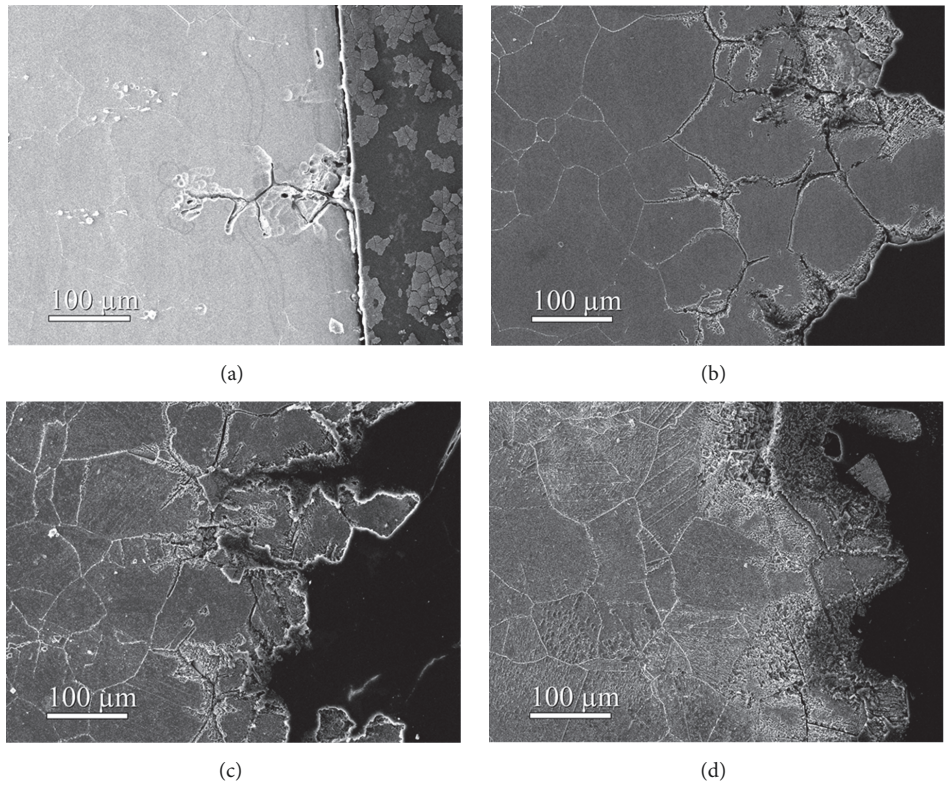

Figure 7: SEM images of the cross-sections in the Alloy 625 after for (a) 0h, (b) 40h (c), (e) 200h, and (d),(f) 1000h after 120 h ferric sulfate-sulfuric acid corrosion test.

alloy's concentration of C_G^0 is interior part; x is distance to grain boundary; D is diffusion coefficient; and t is aging time.

Alloy element of grain boundary precipitation by different sensitization time causes dilution zone's composition change, and qualitative results are shown in Figure 8.

The widths of the depleted zone, $x_{40} = x_{200}/\sqrt{5} = x_{1000}/5$,where in this region complete passivation film cannot be formed, are proportional to the square root of the aging time; that is, the volume of the dilution area follows the parabola law.

As can be seen from Figures 6 and 7, corrosion mainly originated from the carbide and precipitated phases and then gradually expanded into the interior of the grain. When the grain loses its support, it falls off under the action of corrosion. In addition, the volume fraction of precipitated phase increased with the increasing of aging time, leading to the aggravation of corrosion. Therefore, the surface presents a glacial like corrosion appearance because a dense passivation film cannot be formed at δ phase [10, 20]. The corrosion potential of carbides and intermetallic at the grain boundary is relatively low; therefore, preferred dissolution occurs during immersion, as shown in Figure 9.

It can be deduced from the above analysis that the mass loss rate (mpy) is related to the number of precipitated phases [21] and the diffusion of alloy elements. After aging for 200 h, because of the precipitation of needle-like δ phase, the peel off grain and lead to further increases of the mass loss rate. The mass loss rate of the Alloy 625 is not proportional to the square root of aging time especially within 200 hours, which means that the mass loss rate cannot be explained by diffusion theory alone. When the grain boundary is completely dissolved, the grain loses its support and falls off. In the process of corrosion, the mass loss mainly consists of

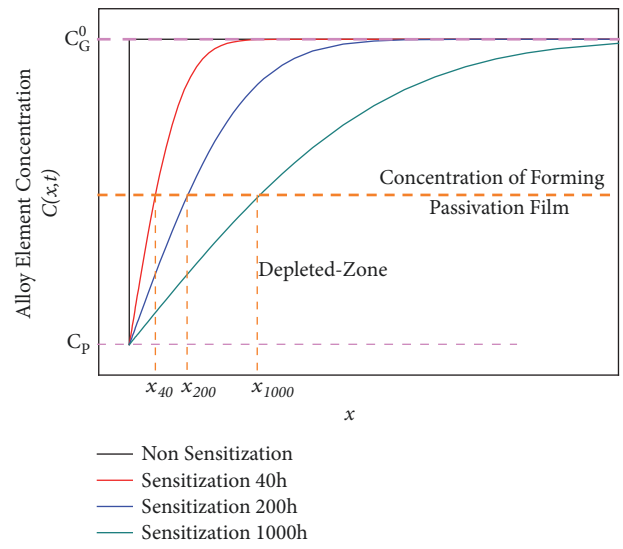

Figure 8: The relationship between aging time and the alloy composition and the width of the depleted zone.

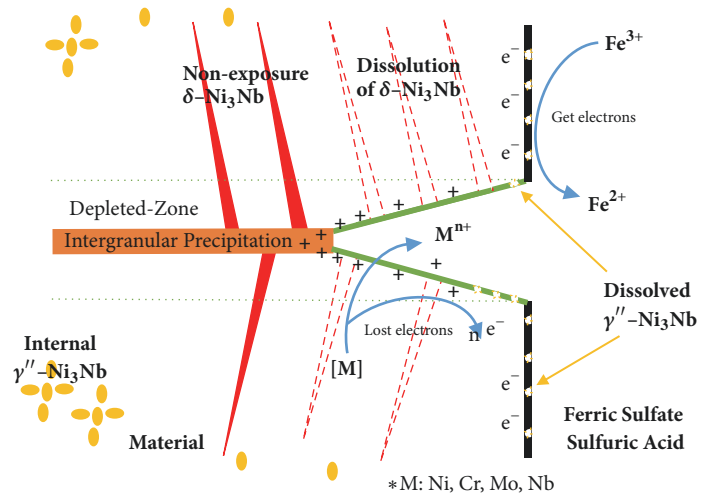

FIGURE 9: Intergranular corrosion mechanism of Inconel 625.

δ phase, grain boundary precipitator, and element dilution area near the grain boundary. The nucleation and growth of the precipitated phase can be characterized by Johnson-Mehl-Avrami (JMA) equations [22–25]:

$$f = 1 - \exp\left(-kt^n\right) \tag{7}$$

where f is volume fraction of precipitation phase; t is the ratio of the volume of the precipitated phase at a certain time to the volume of the precipitated phase at an infinite time; k is time constant associated with temperature; and n is time constant, between 1 and 4.

The volume fraction of element dilution zone and precipitated phase at the grain boundary can be obtained as follows:

$$\begin{aligned} f_{ip} &= 1 - \exp\left(-k_{ip}t^{n_1}\right) \\ f_\delta &= 1 - \exp\left(-k_\delta t^{n_2}\right) \end{aligned} \tag{8}$$

where f_{ip} is volume fraction of precipitation phase and grain boundary element depleted zone and f_δ is volume fraction of needle-like δ phase.

In addition, corrosion rate is as follows:

$$mpy = af_{ip} + bf_\delta + c \quad (mm/a) \tag{9}$$

where a, b, c are constants.

When t =0, mpy = 1.267 (mm/a).

As can be seen from (5) and (6),

$$\begin{aligned} mpy = {} & 44.32\left[1 - \exp\left(-\frac{t}{10.99}\right)\right] \\ & + 44.62\left[1 - \exp\left(-\frac{t}{327.8}\right)\right] \\ & + 1.267 \quad (mm/a) \end{aligned} \tag{10}$$

a = 44.32, b = 44.62, k_{ip} = 1/10.99, k_δ = 1/327.8, n_1 = 1, and n_2 = 1.

5. Conclusion

The effect of aging time on intergranular corrosion behavior of a ultra-low Fe Alloy 625 was investigated by surface observation and immersion testing methods. The deterioration of intergranular corrosion resistance of the tested alloy was discussed. The results are summarized as follows.

(1) The Cr depleted zone is formed around the grain boundary during the aging process. The precipitated phase γ''-Ni_3Nb was mainly precipitated at the grain boundaries and twin boundaries. The number and volume of γ'' increased with the prolonging of aging time. The transformation of γ'' to δ-Ni_3Nb occurred after aging periods of 200 h.

(2) It can be seen that the weight loss during corrosion increases with aging time. The corrosion resistance of Alloy 625 was significantly reduced during aging treatment. The decrease in intergranular corrosion resistance of alloy 625 was attributed to the dissolution of precipitated phase and chromium depleted zone. The mass loss rate is explained by Johnson-Mehl-Avrami equation.

(3) The falling off of grains was due to the dissolution of Cr depleted zone and precipitation phase. The model of intergranular corrosion is established.

Data Availability

All the data in the manuscript is original. All data is only accessible in the manuscript. The data in the text is original, and anyone cannot modify it at will.

Conflicts of Interest

The authors declare that they have no conflicts of interest.

Acknowledgments

The authors are grateful for the financial support by Science and Technology Program of Jiangsu Province (Nos. BE2015144 and BE2015145).

References

[1] S. A. Al-Fozan and A. U. Malik, "Effect of seawater level on corrosion behavior of different alloys," *Desalination*, vol. 228, no. 1–3, pp. 61–67, 2008.

[2] Z. Yin, W. Zhao, W. Lai, and X. Zhao, "Electrochemical behaviour of Ni-base alloys exposed under oil/gas field environments," *Corrosion Science*, vol. 51, no. 8, pp. 1702–1706, 2009.

[3] T. M. Smith, B. D. Esser, N. Antolin et al., "Phase transformation strengthening of high-temperature superalloys," *Nature Communications*, vol. 7, no. 1, 2016.

[4] R. Dutta, "Corrosion aspects of Ni–Cr–Fe based and Ni–Cu based steam generator tube materials," *Journal of Nuclear Materials*, vol. 393, no. 2, pp. 343–349, 2009.

[5] X. Ren, K. Sridharan, and T. R. Allen, "Corrosion Behavior of Alloys 625 and 718 in Supercritical Water," *Corrosion*, vol. 63, no. 7, pp. 603–612, 2007.

[6] V. Shankar, K. Bhanu Sankara Rao, and S. Mannan, "Microstructure and mechanical properties of Inconel 625 superalloy," *Journal of Nuclear Materials*, vol. 288, no. 2-3, pp. 222–232, 2001.

[7] L. M. Suave, D. Bertheau, J. Cormier, P. Villechaise, A. Soula, Z. Hervier et al., "Impact of Thermomechanical Aging on Alloy 625 High Temperature Mechanical Properties," in *8th International Symposium on Superalloy 718 and Derivatives*, pp. 317–331, John Wiley & Sons, Pittsburgh, PA, USA, 2014.

[8] L. M. Suave, J. Cormier, P. Villechaise et al., "Microstructural Evolutions During Thermal Aging of Alloy 625: Impact of Temperature and Forming Process," *Metallurgical and Materials Transactions A: Physical Metallurgy and Materials Science*, vol. 45, no. 7, pp. 2963–2982, 2014.

[9] M. Shaikh, M. Ahmad, K. Shoaib, J. Akhter, and M. Iqbal, " Precipitation hardening in Inconel ," *Materials Science and Technology*, vol. 16, no. 2, pp. 129–132, 2013.

[10] H. M. Tawancy, I. M. Allam, and N. M. Abbas, "Effect of Ni3Nb precipitation on the corrosion resistance of Inconel alloy 625," *Journal of Materials Science Letters*, vol. 9, no. 3, pp. 343–347, 1990.

[11] K. Kaneko, T. Fukunaga, K. Yamada et al., "Formation of M23C6-type precipitates and chromium-depleted zones in austenite stainless steel," *Scripta Materialia*, vol. 65, no. 6, pp. 509–512, 2011.

[12] Y. -. Pan, D. S. Dunn, G. A. Cragnolino, and N. Sridhar, "Grain-boundary chemistry and intergranular corrosion in alloy 825," *Metallurgical and Materials Transactions A: Physical Metallurgy and Materials Science*, vol. 31, no. 4, pp. 1163–1173, 2000.

[13] H. Sahlaoui, H. Sidhom, and J. Philibert, "Prediction of chromium depleted-zone evolution during aging of Ni-Cr-Fe alloys," *Acta Materialia*, vol. 50, no. 6, pp. 1383–1392, 2002.

[14] S. K. B., B. S. Prasad, V. Kain, and J. Reddy, "Methods for making alloy 600 resistant to sensitization and intergranular corrosion," *Corrosion Science*, vol. 70, pp. 55–61, 2013.

[15] L. Yuan, R. Hu, T. Zhang, Y. Han, X. Xue, and J. Li, "Precipitation Behavior of σ-FeCr Phases in Hastelloy C-2000 Superalloy Under Plastic Deformation and Aging Treatment," *Journal of Materials Engineering and Performance*, vol. 24, no. 2, pp. 565–571, 2015.

[16] C. M. Kuo, Y. T. Yang, H. Y. Bor, C. N. Wei, and C. C. Tai, "Aging effects on the microstructure and creep behavior of inconel 718 superalloy," *Materials Science and Engineering: A Structural Materials: Properties, Microstructure and Processing*, vol. 510-511, pp. 289–294, 2009.

[17] K. ke-hsin, "Phases in high alloy steels and superalloys," *Acta Metallurgica Sinica (English Letters)*, vol. 14, pp. 73–95, 1978, http://www.cnki.com.cn/Article/CJFDTotal-JSXB197801008.htm .7395.

[18] Anon, "Standard test methods of detecting susceptibility to intergranular attack in wrought, nickel-rich, chromium-bearing alloys," in *Proceedings of the Laboratory Corrosion Tests and Standards.*, pp. 527–533.

[19] A. Fick, "Ueber diffusion," *Annalen der Physik*, vol. 170, no. 1, pp. 59–86, 1855.

[20] W. Boesch and H. Canada, "Precipitation Reactions and Stability of Ni_3Cb in Inconel Alloy 718," in *Proceedings of the Superalloys*, pp. 579–596, September 1968.

[21] M. Prohaska, H. Kanduth, G. Mori, R. Grill, and G. Tischler, "On the substitution of conventional corrosion tests by an electrochemical potentiokinetic reactivation test," *Corrosion Science*, vol. 52, no. 5, pp. 1582–1592, 2010.

[22] X. Di, X. Liu, C. Chen, B. Wang, and X. Guo, "Effect of Post-weld Heat Treatment on the Microstructure and Corrosion Resistance of Deposited Metal of a High-Chromium Nickel-Based Alloy," *Acta Metallurgica Sinica (English Letters)*, vol. 29, no. 12, pp. 1136–1143, 2016.

[23] M. Avrami, "Kinetics of phase change. I: general theory," *The Journal of Chemical Physics*, vol. 7, no. 12, pp. 1103–1112, 1939.

[24] M. Avrami, "Kinetics of phase change 2," *The Journal of Chemical Physics*, vol. 7, no. 12, pp. 1103–1112, 1939.

[25] W. A. Johnson and R. F. Mehl, "Reaction Kinetics in Process of Nucleation and Growth," *Journal of Chemical Physics*, vol. 8, pp. 212–1112, 1940.